Supporting information

Surface reconstructing hierarchical structures as robust sulfion oxidation catalysts to produce hydrogen with ultralow energy consumption

Taotao Gao,[a] Xiangmin Tang,[b] Xiaoqin Li,[a] Hai Lan,[c] Shumin Yu,[b] Shuaiwei Wu,[b] Qu Yue*[a] and Dan Xiao*[a,d]

a Institute for Advanced Study, Chengdu University, Chengdu, 610106, P. R. China,

E-mail: xiaodan@scu.edu.cn, yuequ@cdu.edu.cn

b School of Mechanical Engineering, Chengdu University, Chengdu, 610106, P. R. China.

c College of Materials Science and Engineering, Chongqing Jiaotong University, Chongqing, 400074, P. R. China.

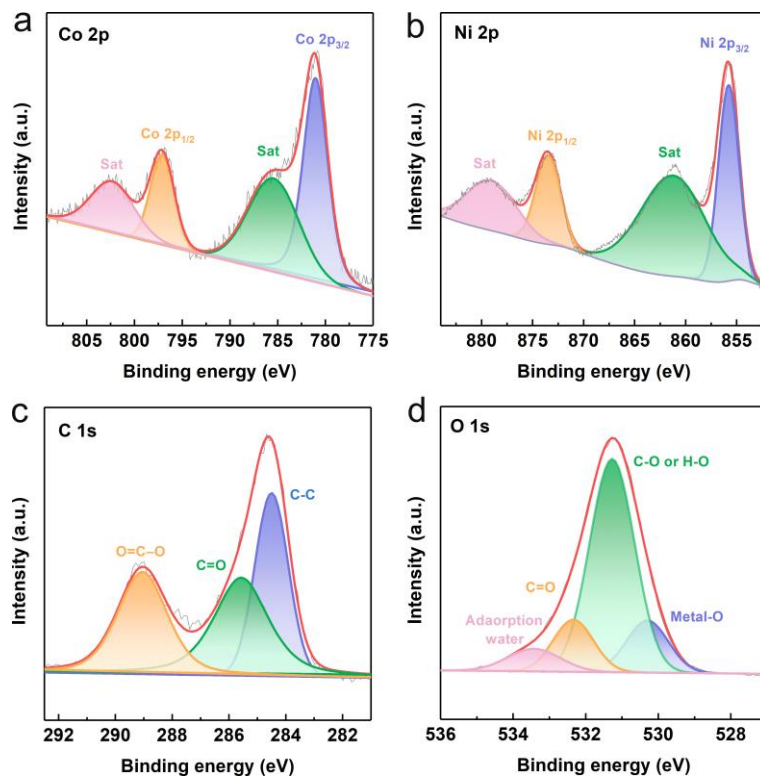d College of Chemical Engineering, Sichuan University, Chengdu, 610065, P. R. China.

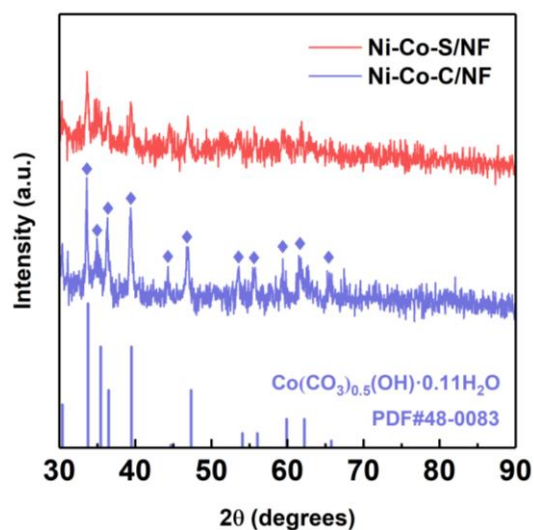**Fig. S1.** The (a) Co 2p, (b) Ni 2p, (c) C1s and (d) O1s spectra of Ni-Co-C/NF.

Fig. S2. XRD patterns of the powder samples scraped from Ni-Co-C/NF and Ni-Co-S/NF, respectively.

Table S1. Ni, Co and S contents in Ni-Co-C/NF and Ni-Co-S/NF based on the ICP-AES experiment.

Samples	Ni (wt.%)	Co (wt.%)	S (wt.%)
Ni-Co-C/NF	5.9	51.5	0.0
Ni-Co-S/NF	4.3	38.8	5.3

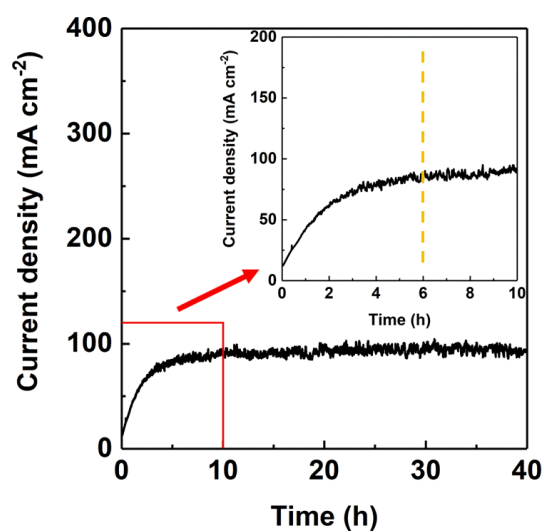**Fig. S3.** The I-t curve during the activation process of Ni-Co-C/NF at the potential of 0.35 V vs. RHE.

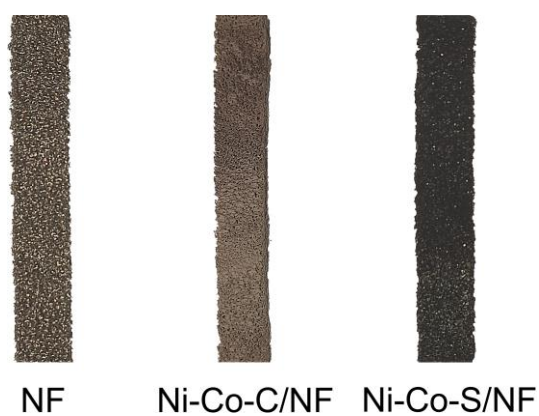NF   Ni-Co-C/NF   Ni-Co-S/NF

Fig. S4. Images of NF (silver gray), Ni-Co-C/NF (pink) and Ni-Co-S/NF (black), respectively.
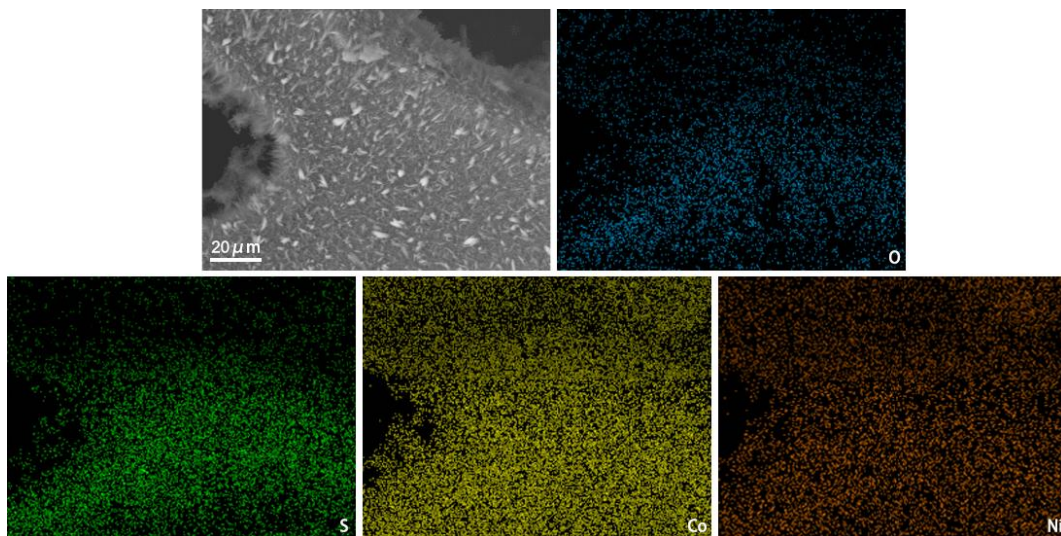
Fig. S5. SEM image of Ni-Co-S/NF and the element mapping of O, S, Co and Ni respectively.
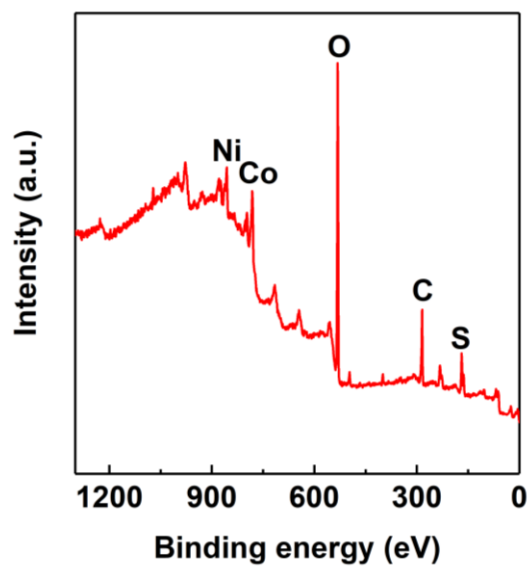

Fig. S6. The XPS full spectrum of Ni-Co-S/NF.
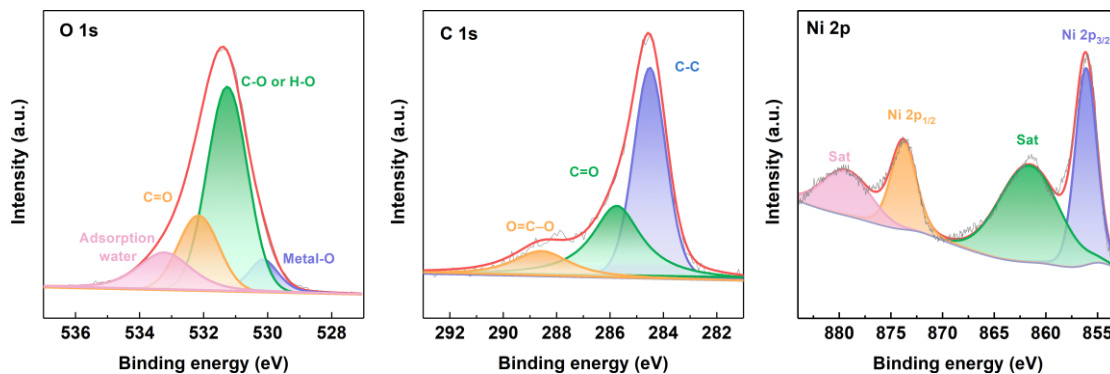
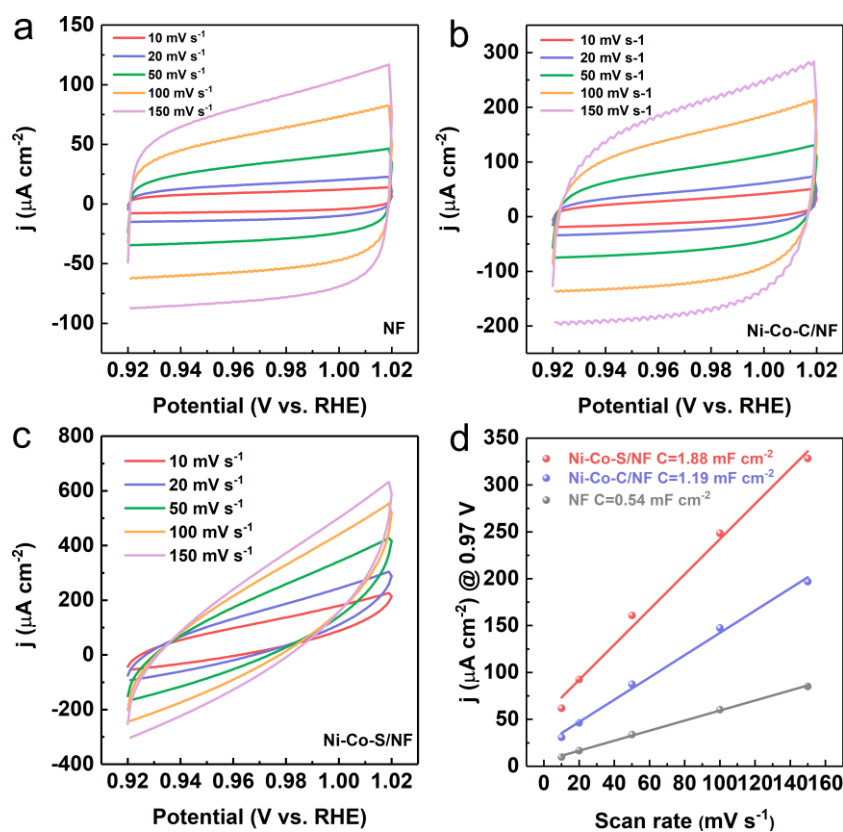**Fig. S7.** The O 1s, C 1s and Ni 2p spectra of Ni-Co-S/NF.

Fig. S8. The double-layer capacitance measurements of the electrodes; a-c) the cyclic voltammograms of the catalysts at a series of scan rates of 10, 20, 50, 100 and 150 mV s^{-1} from 0.92 to 1.02 V vs. RHE in 1 M NaOH; d) the linear fitting of the oxidation currents of the catalysts at 0.97 V vs. RHE versus scan rates.

Electrical double-layer capacitance measurements were used to determine the electrochemical active surface area (ECSA) of the catalysts. According to Fig. S8d, the electrical double-layer capacitance could be obtained based on the specific capacitance value of a smooth standard with a real surface area of 1 cm^{-2}. 40 uF cm^{-2} is considered as the value of specific capacitance for a smooth standard with a real surface area of 1 cm^{-2} based on previous studies.

The electrochemical active surface area could be obtained via the following equation:

$$A_{ECSA} = \frac{\text{The electrical double−layer capacitor}}{40}$$

For example:

Ni-Co-S/NF: $A_{ECSA} = \frac{1880}{40} = 47.00 \text{ cm}^2_{ECSA}$

Table S2. The calculated ECSA of the obtained electrodes.

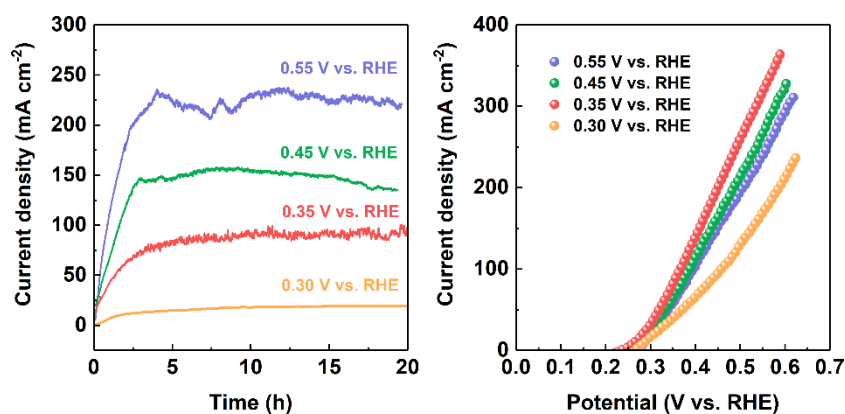| Electrodes	C (mF cm^{-2})	ESCA (cm^2)
NF	0.54	11.25
Ni-Co-C/NF	1.19	29.75
Ni-Co-S/NF	1.88	47.00

Fig. S9. (a) I-t curves of the Ni-Co-C/NF electrodes at different activation potentials and (b) polarization curves of the corresponding Ni-Co-C/NF electrodes.
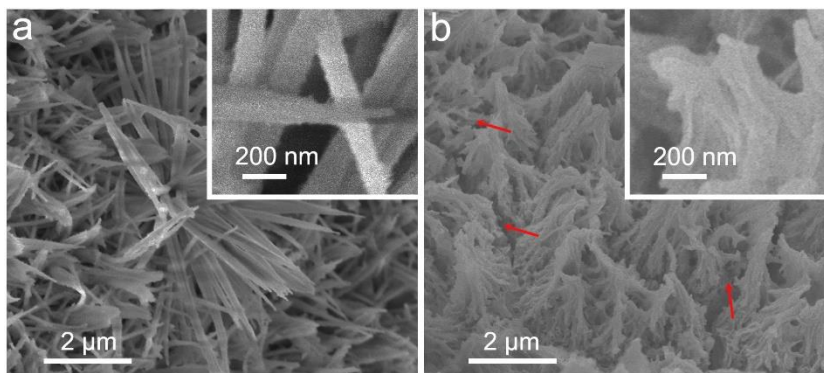
Fig. S10 SEM images of the Ni-Co-S/NF electrodes activated at the potentials of (a) 0.30 V vs. RHE and (b) 0.45 V vs. RHE, respectively.

The different activation potentials would result in differences in morphology and structure, which is closely related to electrochemical performance.[1] Therefore, the SEM test of the Ni-Co-S/NF electrodes prepared at different activation potentials is performed. According to the SEM image of the Ni-Co-S/NF obtained at 0.35 V vs. RHE (Fig. 2c), the surface of needle-like nanorods becomes rough, and the tops of the needle-like nanorods interwoven together to form a stable structure, which is different from the initially smooth surface and relatively independent state (Fig. 2a). However, compared with the electrode activated at 0.35 V vs. RHE, the activation degree of the Ni-Co-S/NF obtained at a lower potential of 0.30 V vs. RHE is inadequate according to the almost smooth surface of the needle-like nanorods (Fig. S10a). Meanwhile, the higher activation potential (0.45 V vs. RHE) leads to the remarkable coalescence and fracture of nanorods (Fig. S10b). Therefore, the Ni-Co-S/NF electrode activated at 0.35 V vs. RHE obtains the optimal activation degree as well as high structure stability, and then displays efficient SOR catalytic activity and robust stability (Fig. 3 and S9).

Table S3. Comparison of SOR catalytic activity.

| Catalysts	Electrolytes	Potential (V) @100 mA cm^{-2}	References
Co-Ni$_3$S$_2$	1 M NaOH+1M Na$_2$S	0.59	[2]
Cu$_2$S/NF	1 M NaOH+1M Na$_2$S	0.44	[3]
WS$_2$ NSs	1 M NaOH+1M Na$_2$S	~0.75	[4]
CoS$_2$@C/MXene/NF	1 M NaOH+1M Na$_2$S	0.389	[5]
VSe$_2$	1 M NaOH+1M Na$_2$S	0.45	[6]
Graphite electrode	1 M NaOH+ 1M NaHS+2 M NaClb	0.51	[7]
Pt disk	1M Na$_2$S	1.0 (vs SCE)	[8]
CoNi@NGs	1 M NaOH+1M Na$_2$S	0.52	[9]
Ni-Co-S/NF	1 M NaOH+1M Na$_2$S	0.366	This work
Ni-Co-C/NF	1 M NaOH+1M Na$_2$S	0.431	This work
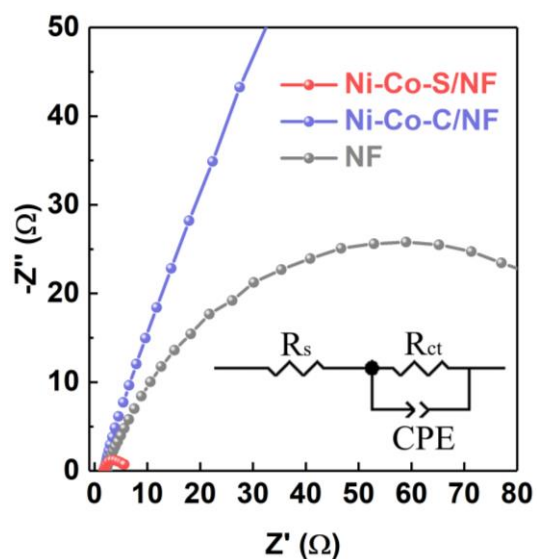
Fig. 11. Electrochemical alternating current impedance of the samples at 0.32 V vs. RHE.
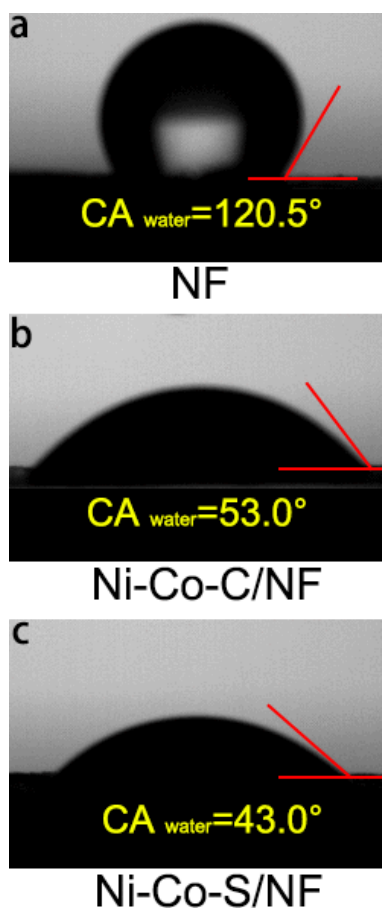

Fig. S12. Contact angle of the aqueous droplet on (a) NF, (b) Ni-Co-C/NF and (c) Ni-Co-S/NF, respectively.
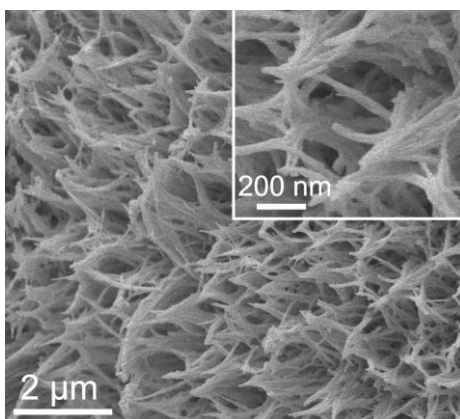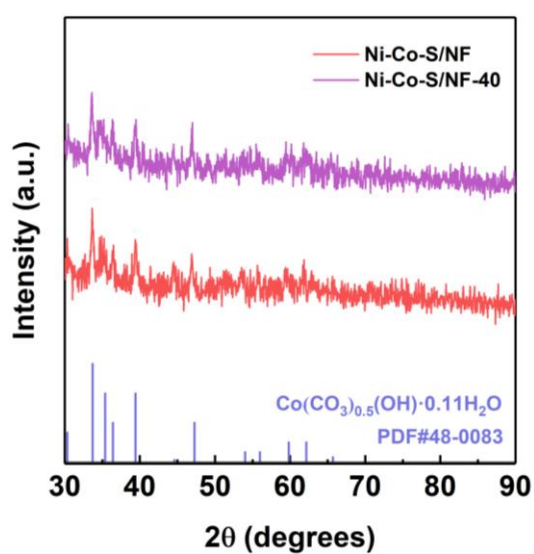
Fig. S13. The SEM images of Ni-Co-S/NF-40.

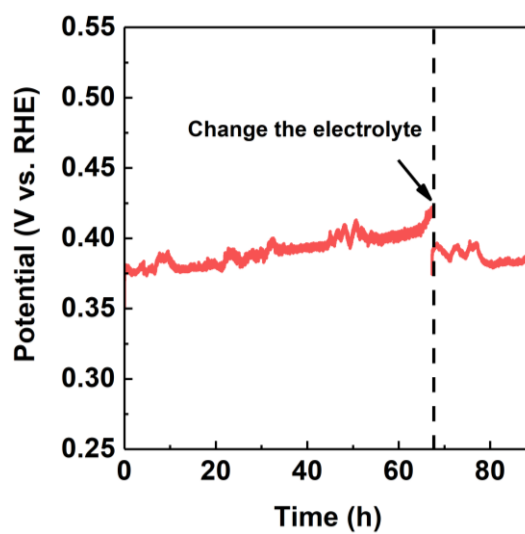**Fig. S14.** The XRD patterns of Ni-Co-S/NF and Ni-Co-S/NF-40.

Fig. S15. The stability test of Ni-Co-S/NF at the current density of 100 mA cm^{-2}.

Table S4. Comparison of the electrochemical hydrogen production performance of the two-electrode electrolytic system.

| Catalysts	Electrolyte	Potential (V) @100 mA cm^{-2}	References
Co-Ni$_3$S$_2$	1 M NaOH+1M Na$_2$S || 1 M NaOH+1M Na$_2$S	0.950	[2]
Cu$_2$S/NF	1 M NaOH+1M Na$_2$S || 1 M NaOH	0.640	[3]
WS$_2$ NSs	1 M NaOH+2 M Na$_2$S || 2.5 M H$_2$SO$_4$	~1.24	[4]
CoS$_2$@C/MXene/NF	1 M NaOH+1M Na$_2$S || Sea water	~0.61	[5]
CoNiCuMnMo-NPs/CC	0.1M KOH+0.1 M MGLY || 0.5 M H$_2$SO$_4$	0.550/-/-	[10]
CC@N-CoP	0.96 M FeSO$_4$/0.74 M Fe$_3$(SO$_4$)$_2$ in 0.5 M H$_2$SO$_4$ || 0.5 M H$_2$SO$_4$	1.18	[11]
Ni-Co-S/NF || Pt-C/CP	1 M NaOH+1M Na$_2$S || 0.5 M H$_2$SO$_4$	-0.274	This work
Ni-Co-S/NF || Pt-C/CP	1 M NaOH+1M Na$_2$S || 1 M NaOH	0.531	This work
Ni-Co-S/NF || Pt-C/CP	1 M NaOH || 0.5 M H$_2$SO$_4$	1.098	This work
Ni-Co-S/NF || Pt-C/CP	1 M NaOH || 1 M NaOH	1.822	This work
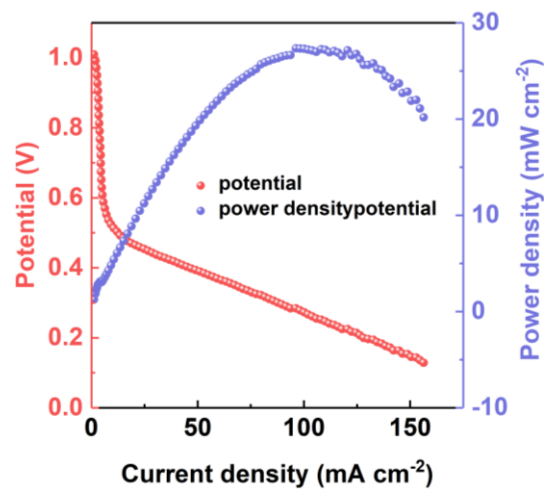
Fig. S16. The polarization curve and corresponding power density of the two-electrode system in a dissymmetrical acid (Pt-C/CP for HER)-base (Ni-Co-S/NF for SOR) coupled electrolyzer (this electrolyzer is used as the galvanic cell at the low current density).

The calculation formula is as follows:

1 Kg H_2 is generated, and the required amount of charge (Q) is:

Q=(1000g×N_A×2e)/M_{H2} = (1000×2×6.022×10^{23}×1.602×10^{-19})/2.016=95706785.7 C

Where N_A is the Avogadro constant, e is the charge of an electron and M_{H2} is the relative molecular mass of hydrogen (H_2).

For the HER (pH=14) + OER (pH=14) system, the applied voltages (U1) at a current density of 100 mA cm^{-2} is 1.822 V. The amount of electricity (W1) required to obtain 1 Kg H_2 is:

W1 = $QU1$ = 95706785.7 ×1.822 = 174377763.545 J ≈48.438 KW·h

For HER (pH=14) + SOR (pH=14) system, the applied voltages (U2) at the current density of 100 mA cm^{-2} is 0.531 V.

The amount of electricity (W2) required to obtain 1 Kg H_2 is:

W2 = $QU2$ = 95706785.7 ×0.531 = 50820303.207 J ≈14.117 KW·h

For HER (pH=0)+OER (pH=14) system, the applied voltages (U3) at the current density of 100 mA cm^{-2} is 1.098 V.

The amount of electricity (W3) required to obtain 1 Kg H_2 is:

W3 = $QU3$ = 95706785.7 ×1.098 = 105086050.698 J ≈29.191 KW·h

For HER (pH=0)+SOR (pH=14) system, the applied voltages (U4) at the current density of 100 mA cm^{-2} is -0.274 V.

The amount of electricity (W3) required to obtain 1 Kg H_2 is:

W4 = $QU4$ = 95706785.7 ×(-0.274) = -26223.659.282 J ≈-7.284 KW·h

Table S5. The energy consumption of different systems to obtain 1 Kg H_2 of different electrolytes in this work.

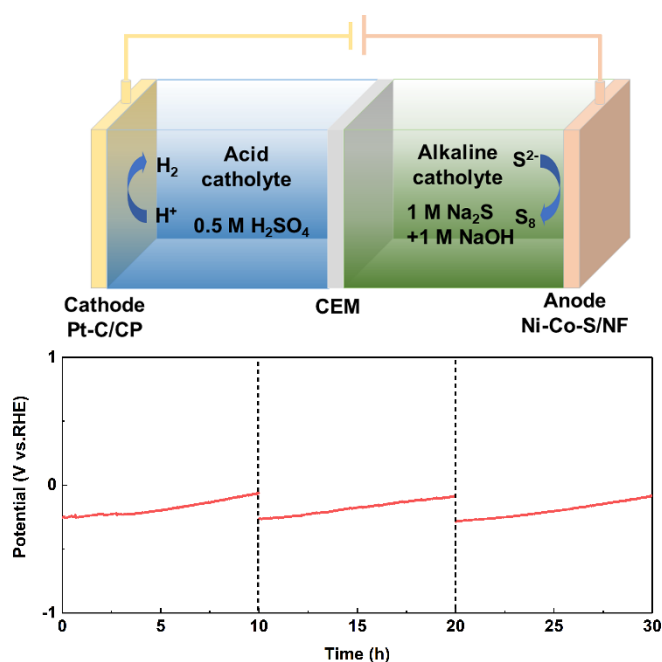| Catalytic electrodes	Voltage (V) @100 mA cm^{-2}	The amount of electricity (KW·h) @ 100 mA cm^{-2}
HER (pH=14) + OER (pH=14)	1.822	48.438
HER (pH=14) + SOR (pH=14)	0.531	14.117
HER (pH=0) + OER (pH=14)	1.098	29.191
HER (pH=0) + SOR (pH=14)	-0.274 (discharge)	-7.284 (discharge)

Fig. S17. (a) the schematic of the electrolyzer and (b) Stability test for the dissymmetrical acid (Pt-C/CP for HER)-base (Ni-Co-S/NF for SOR) coupled system.
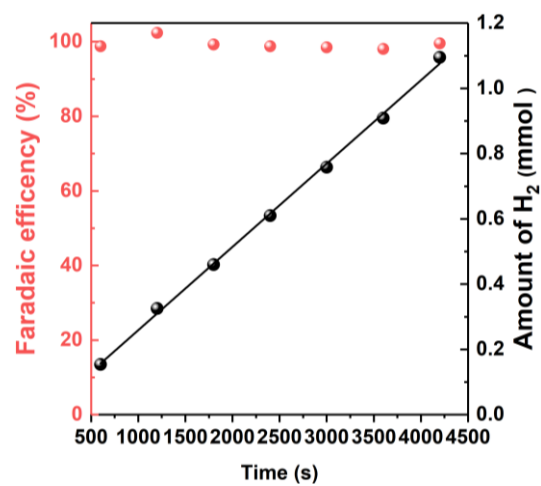
Fig. S18. The Faraday efficiency test for H_2 in the dissymmetrical coupled system based SOR.

Calculation of Faradic efficiency for sulfur: The electrolyte after the electrolysis process is acidified by adding sulfuric acid (the pH value of the electrolyte was adjusted to about 1 to form colloidal sulfur based on equation (1)), centrifuged, washed, dried and then weighed to obtain the weight of the sulfur product. According to equations (1) and (2), S^{2-} is converted into polysulfide (S_x^{2-}) and finally sulfur is formed. No matter what the value of x, the number of transferred electrons (n) in the whole SOR process from S^{2-} to S is 2.

$$S_x^{2-}+H^+\rightarrow(x-1)S+HS^- \quad (1)$$
$$xS^{2-}-2e^-\rightarrow S_x^{2-} \ (x=1\sim8) \quad (2)$$
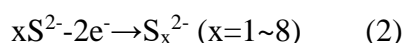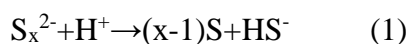
The Faradaic efficiency can be obtained based on the following equations (3) - (5).

$$Q = j \times t \quad (3)$$
$$m_{theory} = \frac{Q \times M_S}{n \times F} \quad (4)$$
$$Faradaic \ efficiency(\%) = \frac{m_S}{m_{theory}} \times 100\% \quad (5)$$

Where Q is the total quantity of electric charge consumed; M_S is the relative molecular weight of S (32); n is the number of transferred electrons in the whole SOR process from S^{2-} to S; F, j and t are the Faraday constant (96485 C mol^{-1}), the current density and reaction time, respectively; m_s and m_{theory} are the practice and theory weight of generated sulfur.

Table S6. Yield of sulfur powder and the faradaic efficiency of SOR.

Time (h)	Practical sulfur powder yield (g)	Theoretical sulfur powder yield (g)	Faradaic efficiency of SOR (%)
0	0	0	0
20	0.568	0.597	95.1
40	1.163	1.195	97.3
60	1.751	1.792	97.7

References

1. Liu, Y.; Jiang, Y.; Hu, Z.; Peng, J.; Lai, W.; Wu, D.; Zuo, S.; Zhang, J.; Chen, B.; Dai, Z.; Yang, Y.; Huang, Y.; Zhang, W.; Zhao, W.; Zhang, W.; Wang, L.; Chou, S., In-Situ Electrochemically Activated Surface Vanadium Valence in V2C MXene to Achieve High Capacity and Superior Rate Performance for Zn-Ion Batteries. *Advanced Functional Materials* **2021,** *31* (8), 2008033.

2. Li, Y.; Duan, Y.; Zhang, K.; Yu, W., Efficient anodic chemical conversion to boost hydrogen evolution with low energy consumption over cobalt-doped nickel sulfide electrocatalyst. *Chemical Engineering Journal* **2022,** *433*, 134472.

3. Pei, Y.; Cheng, J.; Zhong, H.; Pi, Z.; Zhao, Y.; Jin, F., Sulfide-oxidation-assisted electrochemical water splitting for H2 production on a bifunctional Cu2S/nickel foam catalyst. *Green Chemistry* **2021,** *23* (18), 6975-6983.

4. Yi, L.; Ji, Y.; Shao, P.; Chen, J.; Li, J.; Li, H.; Chen, K.; Peng, X.; Wen, Z., Scalable Synthesis of Tungsten Disulfide Nanosheets for Alkali-Acid Electrocatalytic Sulfion Recycling and H2 Generation. *Angewandte Chemie International Edition* **2021,** *60* (39), 21550-21557.

5. Zhang, L.; Wang, Z.; Qiu, J., Energy-Saving Hydrogen Production by Seawater Electrolysis Coupling Sulfion Degradation. *Advanced Materials* **2022,** *34* (16), 2109321.

6. Feng, W.; Cheng, M.; Du, R.; Wang, Y.; Wang, P.; Li, H.; Song, L.; Wen, X.; Yang, J.; Li, X.; He, J.; Shi, J., Gram-Scale Synthesized Two-Dimensional VSe2 and SnSe2 for Ultrahigh Electrocatalytic Sulfion Recycling. *Advanced Materials Interfaces* **2022,** *9* (13), 2200060.

7. Petrov, K.; Srinivasan, S., Low temperature removal of hydrogen sulfide from sour gas and its utilization for hydrogen and sulfur production. *International Journal of Hydrogen Energy* **1996,** *21* (3), 163-169.

8. Zhao, Y.; Wang, S.; Varela, H.; Gao, Q.; Hu, X.; Yang, J.; Epstein, I. R., Spatiotemporal Pattern Formation in the Oscillatory Electro-Oxidation of Sulfide on a Platinum Disk. *The Journal of Physical Chemistry C* **2011,** *115* (26), 12965-12971.

9. Zhang, M.; Guan, J.; Tu, Y.; Chen, S.; Wang, Y.; Wang, S.; Yu, L.; Ma, C.; Deng, D.; Bao, X., Highly efficient H2 production from H2S via a robust graphene-encapsulated metal catalyst. *Energy & Environmental Science* **2020,** *13* (1), 119-126.

10. Fan, L.; Ji, Y.; Wang, G.; Chen, J.; Chen, K.; Liu, X.; Wen, Z., High Entropy Alloy Electrocatalytic Electrode toward Alkaline Glycerol Valorization Coupling with Acidic Hydrogen Production. *Journal of the American Chemical Society* **2022,** *144* (16), 7224-7235.

11. Zhou, Q.; Shen, Z.; Zhu, C.; Li, J.; Ding, Z.; Wang, P.; Pan, F.; Zhang, Z.; Ma, H.; Wang, S.; Zhang, H., Nitrogen-Doped CoP Electrocatalysts for Coupled Hydrogen Evolution and Sulfur Generation with Low Energy Consumption. *Advanced Materials* **2018,** *30* (27), 1800140.